Research Article

elucidated that LPCAT1 increased cell proliferation and invasion, using hepatoma cell lines.

Materials and methods

Clinical specimens

Human HCC tissues, including a boundary region, were excised from resected specimens provided by our institute. A total of 37 samples were obtained from surgical specimens. The clinicopathological characteristics are listed in Table 1. Samples were snap-frozen in liquid nitrogen and stored at −80 °C. The study protocol was approved by the ethical committee of our institute, and all the patients gave informed consent for the procedures.

Imaging mass spectrometry using clinical specimens

The frozen tissues were sliced into 10-μm-thick serial sections; furthermore, for H&E staining, they were sliced into 5-μm-thick sections, using a cryostat (*CM1950, Leica Microsystems, Germany*). The samples for IMS were put onto indium-tin-oxide-coated glass slides (Bruker Daltonics, Germany) and dried at room temperature. The matrix solution was prepared by dissolving 50 mg/ml 2,5-dihydroxybenzoic acid (Bruker Daltonics) in 70% methanol. A thin matrix layer was applied to the surface of the plates as described previously [10]. Mass spectra were acquired using Ultraflex II (Bruker Daltonics). In this analysis, we collected signals between *m/z* 400 and 1000 in positive ion mode. The mechanical resolution was 100 μm × 100 μm. The number of laser irradiations was 200 shots in each spot. Image reconstruction was performed using FlexImaging 2.1 software (Bruker Daltonics). The 100 most intense peaks between HCC and normal parenchyma in a single analysis were compared by principal component analysis (PCA) utilizing ClinProTool 2.2 software (Bruker Daltonics). An alignment of mass spectra from different samples was performed using SpecAlign software (http://physchem.ox.ac.uk/~jwong/specalign/). The peak intensity value of the spectra was normalized by dividing by the total ion current, as previously described [11].

Table 1. Patients clinicopathological features.

Sex	
Male	30
Female	7
Age	68 (45-80)
Etiology	
HBV	7
HCV	25
NBNC*	5
Tumor size (maximum diameter), cm	3.0 (1.3-10)
Tumor number	2 (1-7)
Vascular invasion	
Positive	11
Negative	26
Stage (UICC)	
I	15
II	19
IIIA	3
Differentiation	
Well	11
Moderate	24
Poor	1
α-fetoprotein, ng/ml	337 (2-8989)
PIVKA-II, mAU/ml	419 (15-8830)

NBNC, non-B, non-C hepatitis.
*NBNC contains no alcohol addict.

Identification of biomolecules

Tandem mass spectrometry was performed using QSTAR Elite (Applied Biosystems Inc., Foster City, CA), a hybrid quadrupole/time-of-flight mass spectrometer equipped with an orthogonal MALDI source and a pulsed Nd:YAG. The MS/MS analysis was performed directly on the tissue sections. The data acquisition conditions (i.e., the laser power, collision energy, and the number of laser irradiations) were adjusted to obtain good-quality mass spectra with high intensity and signal-to-noise ratios (S/N) in the fragmented peaks. The MS/MS data were assigned using Nature Lipidomics Gateway (http://www.lipidmaps.org/).

Semi-quantitative RT-PCR

Total RNA was extracted using RNeasy mini kit (QIAGEN, Valencia, CA) for tissue samples and Sepasol I (Nakalai Tesque, Japan) for cells, respectively. The extracted RNAs from tissue samples and cells were reverse-transcribed with SuperScript III (Invitrogen, Carlsbad, CA) and ReverTra Ace (TOYOBO LIFE SCIENCE, Japan), respectively. Each single-stranded cDNA of LPCATs and *GAPDH* was amplified on a GeneAmp PCR System 9700 (Applied Biosystems Inc.). PCR primer sequences and reaction conditions are listed in Supplementary Table 1. The PCR bands were visualized using gel documentation system Printgraph AE6932CP-4 (ATTO, Tokyo, Japan). The signal intensity of each band was digitized as a cumulative density of band area. This digitizing of band signal was easily done with a macro command available in Scion image software version 4.0.3.2 (Scion Corporation, Frederick, MD). Signal intensities of LPCATs of each sample were normalized to those of *GAPDH* of the same sample. We confirmed that *GAPDH* was able to be used as a reference as the difference of *GAPDH* signal between cancer and non-cancer was less than 1.2 and not statistically significant. The data were presented as the ratio of LPCATs and *GAPDH*. We loaded all the samples into one gel for quantitative comparison.

Western blotting

A rabbit polyclonal anti-LPCAT1 antibody (Protein Tech Group, Inc., Chicago, IL), rabbit polyclonal anti-LPCAT4 antibody (Protein Tech Group, Inc.), rabbit monoclonal anti-cytosolic phospholipase $A_2\alpha$ ($cPLA_2\alpha$) antibody (Cell Signaling Technology, Inc., Beverly, MA), rabbit polyclonal anti-Ca^{2+}-independent phospholipase A_2 β ($iPLA_2\beta$) antibody (Abcam, UK), mouse monoclonal anti-GAPDH antibody (Millipore Corporate, Billerica, MA), and mouse monoclonal anti-FLAG M2 antibody (Agilent Technology, Santa Clara, CA) were used. The immunoreactive bands were visualized using ECL plus Western Blotting Detection Reagents (GE Healthcare, UK) and an Imaging Reader LAS-3000 mini (FUJIFILM, Japan). We checked the band of LPCAT1 and 4 detected with knockdown samples. We observed that in knockdown samples, the specific band was absent. The evaluation was carried out by quantifying the signal intensity of visible bands with Scion image software.

Cell lines

HCC cell lines HuH7 and HepG2 cells were purchased from Human Science Research Resources Bank (Japan). They were cultured under Dulbecco's modified Eagle's medium (Invitrogen) with 10% fetal bovine serum, 100 U penicillin, and 0.1 mg/ml streptomycin at 37 °C in 5% CO_2.

Small interfering RNA inhibition assay

To knock down endogenous LPCAT1 expression in HuH7 and HepG2 cells, we used Stealth RNAi (Invitrogen). We used Stealth RNAi Negative Control Medium GC Duplex #2 (Invitrogen) as a negative control. HuH7 and HepG2 cells were seeded and transfected with Lipofectamine 2000 (Invitrogen), according to the manufacturer's instructions. The HuH7 and HepG2 cells were harvested 4 days and 3 days after transfection, respectively.

Expression plasmids

The full-length cDNA encoding human *LPCAT1* was purchased from DNAFORM (Japan). The full-length cDNA was amplified using the following primers: sense, 5′-gggGGATCCatgaggctgcggggatgcg and antisense, 3′-gggGAATTCctaatccagcttcttgcgaaca. The amplified fragments were cloned into pCMV-Tag2 vector (Agilent Technologies, Inc.) at *Bam*HI-*Eco*RI sites. All DNA sequences were verified

Please cite this article in press as: Morita Y et al. Lysophosphatidylcholine acyltransferase 1 altered phospholipid composition and regulated hepatoma progression. J Hepatol (2013), http://dx.doi.org/10.1016/j.jhep.2013.02.030

using genetic analyzer ABI PRISM® 3100 (Applied Biosystems Inc.). HuH7 and HepG2 cells were harvested 48 h after transfection with Lipofectamine 2000. pCMV-Tag3c vector (Agilent Technologies, Inc.) was used as a negative control.

Imaging mass spectrometry using carcinoma cell lines

1×10^5 HuH7 and 1.5×10^5 HepG2 cells after transfection were seeded on the ITO slide glass with 8 well FlexiPERM (Greiner Bio-one, Germany) and incubated at 37 °C in 5% CO_2 for 12 h. Then, the medium was removed and the wells were washed three times using 0.1 M phosphate buffer. After drying, a thin matrix layer was applied using matrix sublimation equipment RK27-4069 (Shimadzu Corp, Japan) according to the manufacturer's protocol. Mass spectra were acquired using Ultraflex II. The raster width was 50 μm × 50 μm and the number of laser irradiations was 200 shots in each spot. The 100 most intense peaks acquired from 1500 irradiation points were compared using ClinProTool 2.2 software. The cell confluency was evaluated by the 200× magnified images with Scion image software.

Cell proliferation assay

In knockdown experiments, 2×10^3 HuH7 cells and 4×10^3 HepG2 cells were plated in 96-well plates. Cell proliferation was measured at 3 and 5 days after completion of knockdown. In overexpression experiments, 4×10^3 cells were plated in 96-well plates. Cell proliferation was measured at 2 and 4 days after transfection. MTT Cell Growth Assay Kit (Millipore Corporation) was used according to manufacturer's instructions. The absorbance for live cells was measured with Synergy HT Multi-Mode Microplate Reader (BioTek, Winooski, VT). Analysis was performed on 12 independent wells for each condition and the experiments were repeated three times.

Cell migration and invasion assay

The *in vitro* migration and invasion activities of cells were evaluated using Cell Culture Insert and Matrigel invasion chamber (Becton Dickinson, Bedford, MA) separated by an 8 mm-pore filter membrane. 4×10^4 HuH7 cells and 1×10^5 HepG2 cells in 0.5 ml of serum-free medium were seeded on the upper chamber, and the lower chamber was loaded with 0.75 ml medium with 10% fetal bovine serum. After cultivation for 48 h, cells passed through the membrane were stained with Diff Quik solution (International Reagents, Japan) and counted under an optical microscope, in five randomly selected 100× magnification fields for one membrane. We used three wells for each condition in one experiment.

Statistical analysis

Statistical analyses were performed with Stat View software (version 5.0; Abacus Concepts, Inc., Berkeley, CA) and ClinProTool 2.2 software. Wilcoxon signed-rank test was used for comparison of the measurable variants of two groups. Analysis of variance and Fisher's protected least significant difference tests were performed as *post hoc* tests for the comparison of measurable variants of three or more groups. $p < 0.05$ was defined as statistically significant.

Results

IMS revealed the alteration of phospholipid composition in HCC

We performed IMS of the boundary area containing both cancer and normal liver parenchyma in the HCC tissue sample (Fig. 1A). Mass spectra acquired from cancer tissue seemed to be different from those of the normal liver parenchyma at various *m/z* values (Supplementary Fig. 1A). Unsupervised multivariate analysis, PCA, was performed to identify the different peaks between cancer region and normal region. PCA revealed that the spectra acquired from HCC were quite different from those of the non-cancerous region on the first principal component (Supplementary Fig. 1B). The corresponding loading plot showed the influence of the *m/z* value on the respective principal components (Supplementary Fig. 1C). Subsequently, we performed MS/MS analyses of the detected signals and identified 19 biomolecules with the exception of isotopic data (Table 2). They were composed of 2 lysophosphatidylcholines (LPCs) (No. 1 and 2 in Supplementary Fig. 1C), 13 phosphatidylcholines (PCs) (No. 5–17), 2 triglycerides (No. 18 and 19), 1 sphingomyelin (No. 4), and 1 Heme (No. 3). In particular, *m/z* 770.4 (PC (16:0/16:1), No. 5 in Supplementary Fig. 1C) was one of the most influential peaks on the first principle component. Actually, PC (16:0/16:1) was abundant in the cancerous region from the IMS result (Fig. 1B, middle panel). Meanwhile, LPC (16:0) was scarce in the cancerous region (Fig. 1B, left panel). We normalized the

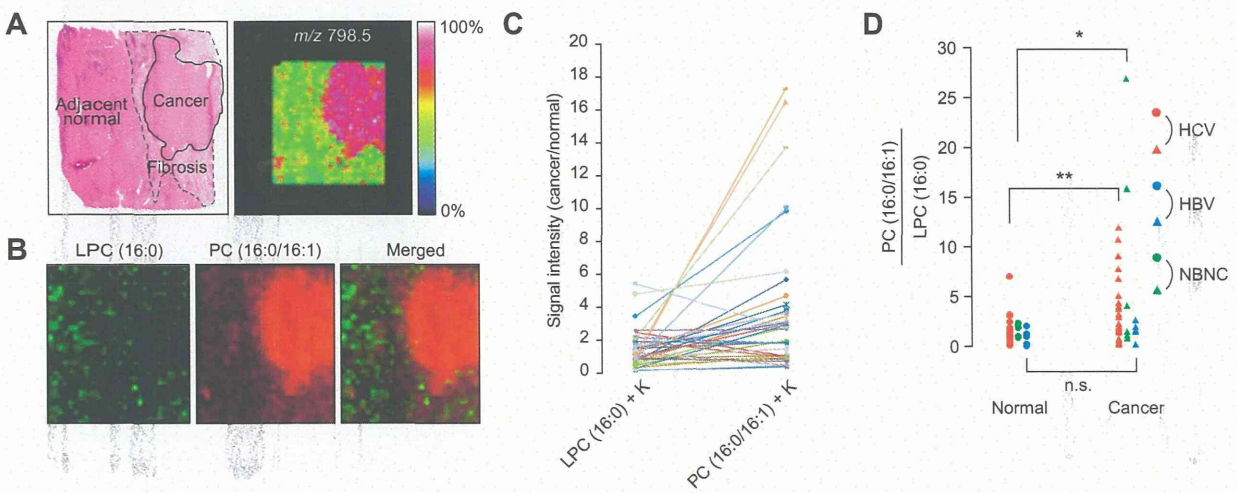

Fig. 1. Imaging mass spectrometry using HCC tissue sample and quantitative analyses of signal intensities in PC and LPC species. (A) Representative histologic finding (H&E staining) and its IMS image at *m/z* 798.5 of HCC tissue sample are shown in the left and right panel, respectively. (B) Reconstructed images acquired from IMS. LPC (16:0): green, PC (16:0/16:1): red, and the merged image are shown. (C) Cancer-to-normal ratios in LPC (16:0) and PC (16:0/16:1) in 37 HCC tissue samples. (D) PC (16:0/16:1)-to-LPC (16:0) ratios in 37 HCC tissue samples. *$p < 0.05$; **$p < 0.01$; n.s., not significant.

Please cite this article in press as: Morita Y et al. Lysophosphatidylcholine acyltransferase 1 altered phospholipid composition and regulated hepatoma progression. J Hepatol (2013), http://dx.doi.org/10.1016/j.jhep.2013.02.030

Research Article

Table 2. The list of biomolecules identified by MS/MS analysis.

No.	Common name	Formula	Calculated mass	Observed mass	Delta	Adduct
1	LysoPC (16:0)	C24H50NO7P	534.2956	534.2930	0.0026	M + K
2	LysoPC (18:0)	C26H54NO7P	562.3269	562.3111	0.0158	M + K
3	Heme B	C34H32O4N4Fe	616.1773	616.1737	0.0036	M + H
4	SM (d18:0/16:1)	C39H79N2O6P	725.5568	725.5499	0.0069	M + Na
5	PC (16:0/16:1)	C40H78NO8P	770.5096	770.4028	0.1068	M + K
6	PC (18:1/18:1)	C44H84NO8P	786.5934	786.4791	0.1143	M + H
7	PC (16:0/18:2)	C42H80NO8P	796.5252	796.5214	0.0038	M + K
8	PC (16:0/18:1)	C42H82NO8P	798.5409	798.5348	0.0061	M + K
9	PC (16:0/20:4)	C44H80NO8P	820.5252	820.5219	0.0033	M + K
10	PC (18:1/18:2)	C44H82NO8P	822.5409	822.4802	0.0607	M + K
11	PC (18:0/18:2)	C44H84NO8P	824.5565	824.4588	0.0977	M + K
12	PC (18:0/18:1)	C44H86NO8P	826.5722	826.4737	0.0985	M + K
13	PC (18:2/20:4)	C46H80NO8P	828.5513	828.4791	0.0722	M + Na
14	PC (18:1/20:4)	C46H82NO8P	846.5409	846.4841	0.0568	M + K
15	PC (18:0/20:4)	C46H84NO8P	848.5565	848.5053	0.0512	M + K
16	PC (18:1/22:6)	C48H82NO8P	870.5409	870.4749	0.0660	M + K
17	PC (18:0/22:6)	C48H84NO8P	872.5565	872.4901	0.0664	M + K
18	TG (16:0/18:1/18:2)	C55H100O6	895.7151	895.7016	0.0135	M + K
19	TG (52/2)	C55H102O6	897.7307	897.7282	0.0025	M + K

Each No. is identical to the number in PCA (Supplementary Fig. 1C).
The common name, formula, and calculated mass were acquired from Nature Lipidomics Gateway and HMBD.
Delta means the difference between calculated mass and observed mass.
Adduct means adductive ions such as H, Na, and K to original molecules (M).

spectra acquired from 37 samples using total ion current with SpecAlign software, and quantified the signal intensity of each biomolecule. The signal intensity of PC (16:0/16:1) was significantly higher in the cancerous region than in the normal region (Fig. 1C). Furthermore, the calculated PC-to-LPC ratios, such as PC (16:0/16:1)/LPC (16:0) in the HCV-related and non-virus-related cancer region, were significantly higher than those in the normal region. PC (16:0/18:1)/LPC (16:0) and PC (18:0/18:1)/LPC (18:0) in the HCV-related cancer region were significantly higher than those in the normal region (p <0.05, Fig. 1D and Supplementary Fig. 2).

LPCAT1 mRNA and protein are highly expressed in HCC

We hypothesized that the alteration of PC-to-LPC ratios in HCC was caused by the increase of specific PC formation from LPC. The homeostasis of phospholipid composition is mainly balanced by LPCATs and PLA_2s. Initially, we investigated the expression level of four LPCATs, which were responsible for LPC to PC conversion, using the RNA extracted from 18 tissue samples (12 HCV-related, 3 HBV-related, and 3 non-virus-related, Fig. 2A). *LPCAT1* and *LPCAT4*, but not *LPCAT2* and *LPCAT3*, were highly expressed in cancers (*LPCAT1*, p <0.01; *LPCAT4*, p <0.05). We further found the significantly higher expression of LPCAT1 protein in HCC (Fig. 2B, p <0.01). Furthermore, the expression level of LPCAT1 protein correlated well with the signal intensity of PC (16:0/16:1) (Fig. 2C). Meanwhile, the expression level of $cPLA_2\alpha$ and $iPLA_2\beta$, which were the candidates to maintain phospholipid composition [12], were not different between the HCC and normal region (Supplementary Fig. 3).

LPCAT1 knockdown changed the PC composition in hepatoma cell lines

We performed an *in vitro* knockdown experiment to investigate the influence of LPCAT1 on PC compositions using two HCC cell lines, HuH7 and HepG2. Fig. 3 and Supplementary Fig. 4 represent the data obtained from the experiments using HuH7 and HepG2 cells, respectively. In both cell lines, reductions in LPCAT1 mRNA and protein were observed after transfection with *LPCAT1*-targeting siRNA compared with an unsilencing siRNA (Fig. 3A, Supplementary Fig. 4A). We confirmed the reduction of some PCs, such as PC (16:0/16:1), after LPCAT1 knockdown using IMS (Fig. 3B and Supplementary Fig. 4B, left and lower panels) in the comparable condition of confluency (Fig. 3B and Supplementary Fig. 4B, right panel). In HuH7 cells, we could detect the alteration of signal intensity relative to that in the control group in six PC species (Fig. 3C). In HepG2 cells, we could detect the alteration of signal intensity in five PC species (Supplementary Fig. 4C).

LPCAT1 knockdown reduced cell proliferation, migration and invasion

We further investigated the influence of LPCAT1 in cell proliferation. LPCAT1 knockdown (siRNA1 and siRNA3) significantly reduced cell proliferation both 3 and 5 days after completion of knockdown in both HuH7 and HepG2 cells (Table 3). Next, we examined the effect of LPCAT1 knockdown on cell migration and invasion. Both the migration and invasion were significantly inhibited after knockdown of LPCAT1 (Table 4).

Please cite this article in press as: Morita Y et al. Lysophosphatidylcholine acyltransferase 1 altered phospholipid composition and regulated hepatoma progression. J Hepatol (2013), http://dx.doi.org/10.1016/j.jhep.2013.02.030

JOURNAL OF HEPATOLOGY

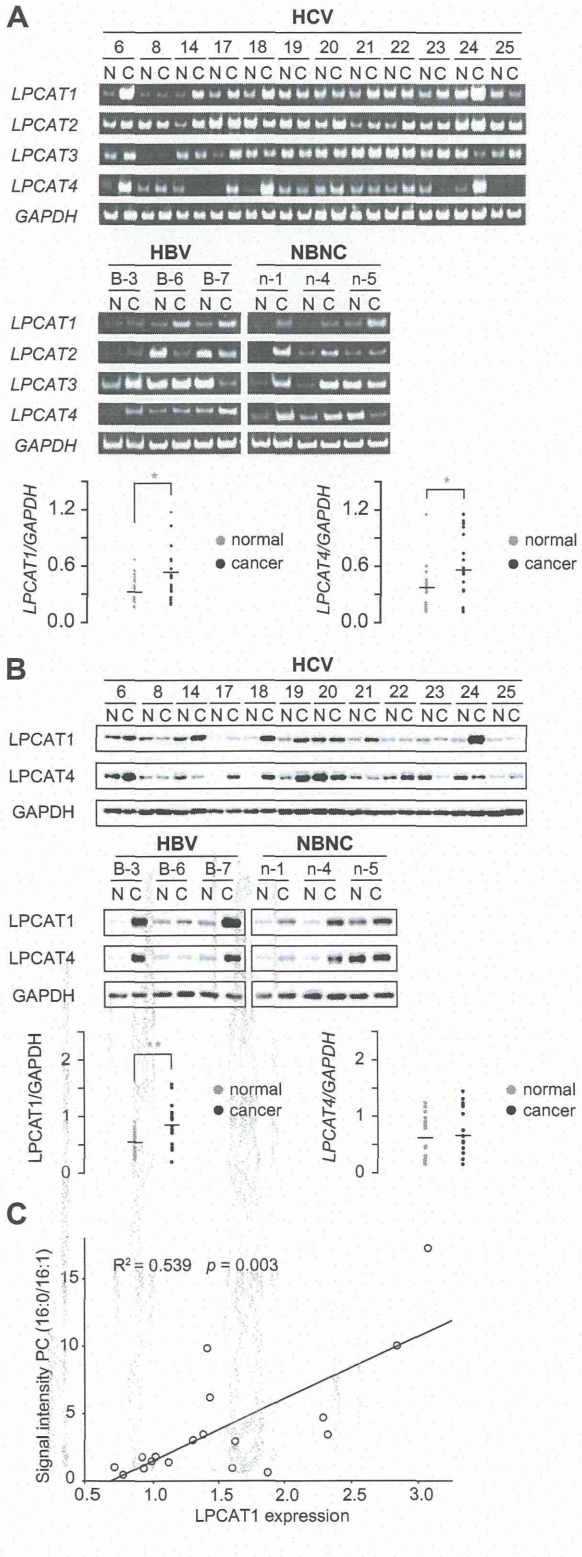

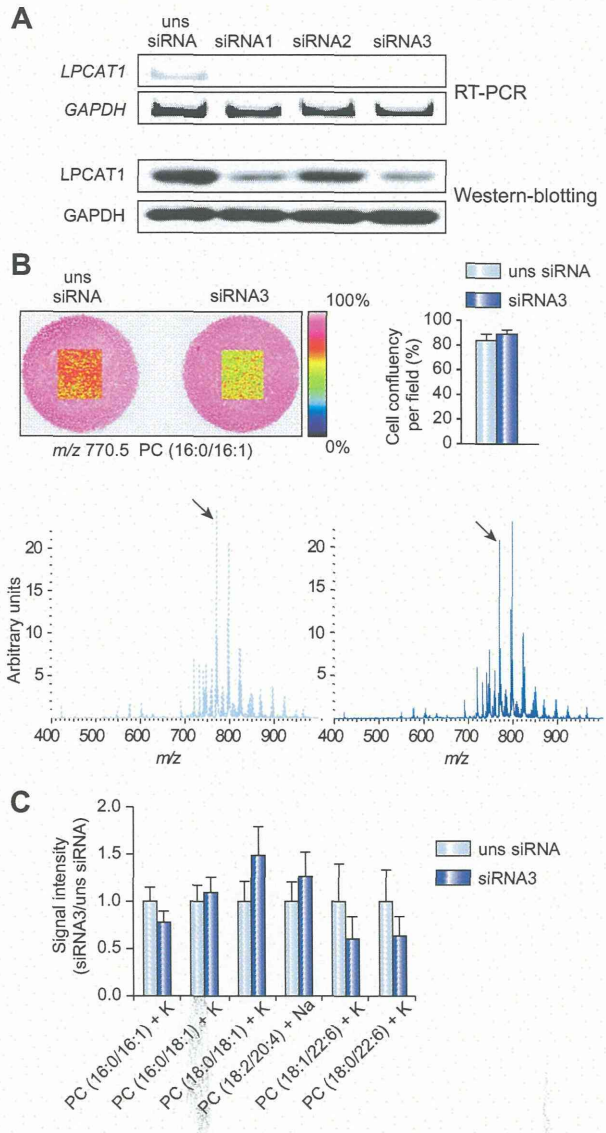

Fig. 3. LPCAT1 knockdown changes PC composition. (A) RT-PCR (upper panel) and Western blotting (lower panel) using HuH7 cells transfected with siRNA to *LPCAT1*, as well as an unsilencing (uns) siRNA. (B) IMS images of PC (16:0/16:1) at *m/z* 770.5 are shown in squares. The color gradient bar indicates the relative intensity. The upper right panel shows the cell confluency for 200× magnified fields. Lower panels show the mass spectra acquired from IMS. The arrows indicate the peaks of PC (16:0/16:1) at *m/z* 770.5. Values are mean ± SD (n = 5). (C) Significantly altered PC species in 3 independent experiments are shown. Values are mean ± SD (n = 1500).

Fig. 2. RT-PCR and Western blotting using HCC tissue extracts. (A) Semiquantitative RT-PCR analyses of *LPCAT1-4* in 12 HCV, 3 HBV, and 3 non-virus-related HCCs. N and C represent adjacent normal parenchyma and cancer tissue, respectively. The experiments were repeated twice. (B) Western blotting analyses of LPCAT1 and LPCAT4 proteins. The experiments were repeated three times. In both panels (A) and (B), lower panels show the densitometric quantification of signal intensities using GAPDH as internal standard. The horizontal line represents the median value (n = 18); $^{*}p < 0.05$; $^{**}p < 0.01$. (C) Correlation between expression level of LPCAT1 protein (*x*-axis) and signal intensity of PC (16:0/16:1) (*y*-axis) is shown.

Please cite this article in press as: Morita Y et al. Lysophosphatidylcholine acyltransferase 1 altered phospholipid composition and regulated hepatoma progression. J Hepatol (2013), http://dx.doi.org/10.1016/j.jhep.2013.02.030

Research Article

Table 3. LPCAT1 knockdown or overexpression affected cell proliferation.

	Cell proliferation (absorbance 570-630 nm)			
	HuH7		HepG2	
	Day 3	Day 5	Day 3	Day 5
Control siRNA				
uns siRNA	0.096 ± 0.011	0.135 ± 0.013	0.409 ± 0.025	0.839 ± 0.043
LPCAT1-siRNA				
siRNA1	0.079 ± 0.008**	0.127 ± 0.010**	0.364 ± 0.021**	0.790 ± 0.097
siRNA3	0.041 ± 0.005**	0.082 ± 0.017**	0.304 ± 0.020**	0.740 ± 0.050**
	Day 2	Day 4	Day 2	Day 4
Control vector				
pCMV-Tag3c	0.266 ± 0.028	0.294 ± 0.042	0.170 ± 0.020	0.226 ± 0.024
LPCAT1-overexpression				
pCMV-Tag2-*LPCAT1*	0.298 ± 0.028**	0.309 ± 0.031	0.182 ± 0.022	0.312 ± 0.029**

Values are mean ± SD (n = 12).
**p <0.01.
uns, unsilencing.

Overexpression of LPCAT1 changed the PC composition in hepatoma cell lines

Next, we generated the CMV-driven mammalian expression vector (pCMV-Tag2-LPCAT1) to investigate the effect of LPCAT1 overexpression on PC compositions. Fig. 4 and Supplementary Fig. 5 represent the data obtained from the experiments using HuH7 and HepG2 cells, respectively. Following expression of this plasmid, a significant increase of LPCAT1 protein was found in Western blotting and immunofluorescent analysis (Fig. 4A and Supplementary Fig. 5A). We confirmed the increase of some PCs, such as PC (16:0/16:1), after LPCAT1 overexpression using IMS (Fig. 4B and Supplementary Fig. 5B, left and lower panels) in comparable conditions of confluency (Fig. 4B and Supplementary Fig. 5B, right panel). In HuH7 cells, we could detect the alteration of signal intensity relative to that in the control group in six PC species (Fig. 4C). In HepG2 cells, we could detect the alteration of signal intensity in seven PC species (Supplementary Fig. 5C).

LPCAT1 overexpression accelerated cell proliferation and invasion

LPCAT1 overexpression significantly increased cell proliferation 2 days after transfection in HuH7 cells. In HepG2 cells, LPCAT1 overexpression significantly increased cell proliferation 4 days after transfection (Table 3). Finally, we examined the effect of LPCAT1 overexpression on cell migration and invasion. The invasion capacity was significantly enhanced after transfection in both HuH7 cells and HepG2 cells (Table 4). On the other hand, the migration ability was not affected in these experiments.

Table 4. LPCAT1 knockdown or overexpression affected cell migration and invasion.

	HuH7	HepG2
Migrated cells per field (cell migration)		
Control siRNA		
uns siRNA	297 ± 119	289 ± 120
LPCAT1-siRNA		
siRNA3	210 ± 78**	132 ± 49**
Control vector		
pCMV-Tag3c	143 ± 51	37 ± 34
LPCAT1-overexpression		
pCMV-Tag2-*LPCAT1*	140 ± 58	42 ± 40
Invaded cells per field (cell invasion)		
Control siRNA		
uns siRNA	102 ± 55	173 ± 130
LPCAT1-siRNA		
siRNA3	22 ± 11**	76 ± 59**
Control vector		
pCMV-Tag3c	48 ± 18	11 ± 11
LPCAT1-overexpression		
pCMV-Tag2-*LPCAT1*	76 ± 48**	22 ± 21**

Values are mean ± SD (n = 15).
**p <0.01.
uns, unsilencing.

Discussion

Aberrant lipid synthesis pathways are thought to be involved in HCC pathophysiology. In this study, we investigated the lipid distribution and composition in clinical HCC samples. IMS revealed that monounsaturated fatty-containing PCs were abundant in HCC. This is in agreement with the literature, which reports an increased ratio of monounsaturated to saturated fatty acids in livers of mice prone to HCC development [13]. Furthermore, palmitoyl acid-containing LPC was scarce in cancerous regions. An additional observation was the paucity of polyunsaturated or highly unsaturated fatty acid-containing PCs in HCC areas (not shown), which concurs with literature reports of omega-3 fatty acids inhibiting the growth of HCC [14]. Taken together, our results suggest that selective changes in the PC and LPC composition promote HCC progression.

Phospholipids are formed from glycerol 3-phosphate by the *de novo* pathway or by remodeling the existing PC species. The *de novo* pathway was originally described by Kennedy and Weiss [15]. Saturated and monounsaturated fatty acids are usually esterified at the *sn-1*-position, whereas unsaturated acyl groups are esterified at the *sn-2*-position. This diversity and asymmetry are not fully explained by the Kennedy pathway. The remodeling

Cancer

Please cite this article in press as: Morita Y et al. Lysophosphatidylcholine acyltransferase 1 altered phospholipid composition and regulated hepatoma progression. J Hepatol (2013), http://dx.doi.org/10.1016/j.jhep.2013.02.030

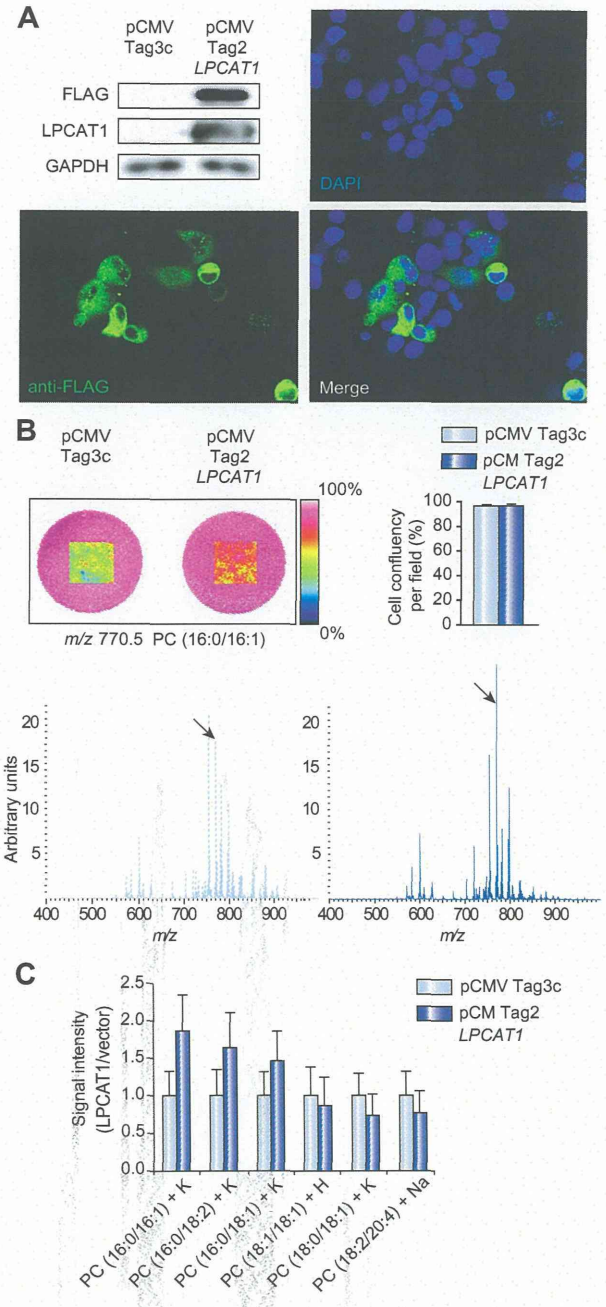

Fig. 4. LPCAT1 overexpression also changed PC composition. (A) Western blotting using anti-FLAG and anti-LPCAT1 antibodies, on lysates from HuH7 cells transfected with pCMV-FLAG-*LPCAT1* and control vector (pCMV-Tag3c). FLAG-tagged LPCAT1 protein was immunofluorescently detected by anti-FLAG antibody in the cytoplasm (green). Nuclei stained with DAPI are in blue (original magnification 400×). Both experiments were performed 2 days after transfection. (B) IMS images at *m/z* 770.5 (PC (16:0/16:1)) 2 days after transfection. The upper right panel shows the confluency at that time point. (C) Significantly altered PC species in 3 independent overexpression experiments are shown. Values are mean ± SD (n = 1500).

pathway (Lands cycle) contributes to achieve a variety of PC species [16]. Lands cycle is mainly regulated by LPCAT and PLA_2. To date, 4 LPCAT subtypes, responsible for LPC to PC conversion, have been identified and each LPCAT has different substrate specificities [17].

We hypothesized that the altered PC composition in HCC was caused by the specific LPCAT overexpression and revealed that LPCAT1 was significantly upregulated in HCCs. LPCAT1 is abundantly expressed in the lung and has been reported to play a fundamental role in the biosynthesis of surfactant dipalmitoyl phosphatidylcholine (DPPC) [18]. Furthermore, LPCAT1 acylates unsaturated acyl groups to maintain cellular membrane integrity [19]. In terms of the substrate specificity of LPCAT1, it seems to be partially identical to the IMS results. Meanwhile, we could not detect the signals corresponding to DPPC, which was thought to be closely related to LPCAT1. This may be due to DPPC accounting for only a small fraction of membrane phospholipid in the mammalian liver [20,21]. Further research is necessary to clarify more precisely the molecular mechanism that determines the whole PC composition.

In the *in vitro* knockdown and overexpression experiments, PC composition could be changed according to LPCAT1 expression. Although LPCAT1 has not been investigated in terms of whether there is a preference for palmitoleoyl-CoA (C16:1), our results suggest that LPCAT1 also has selectivity for palmitoleoyl-CoA as substrate. The affected PCs were partly different between HuH7 and HepG2, suggesting that other unknown factors exist in the homeostasis of PCs in living cells.

The alterations of membrane phospholipid levels can influence cell proliferation and viabilities [22]. Mansilla *et al.* reported on LPCAT1 overexpression in human colorectal cancer [23]. Rapid turnover of membrane PC composition is thought to be required for rapid growth during tumor development. The alterations of membrane phospholipid levels also influence membrane fluidity and facilitate metastases because they affect motility, basement membrane invasion, and adhesion [24]. LPCAT1 also has lyso-platelet activating factor (PAF) acyltransferase activity [25]. PAF significantly induced cell proliferation and invasion in PAF receptor-positive cells [26]. Although LPCAT1 only shows lyso-PAF acyltransferase activity in a quite high concentration of acetyl-CoA, PAF may affect the results to some extent.

The major risk factors of HCC, such as HCV, HBV, and NAFLD, influence lipid metabolism in different ways [27–29]. Keratinocyte growth factor, which stimulates LPCAT1 expression, was reported to increase in chronic liver diseases, in HBV, alcoholic liver disease, and HCV [30,31]. In HCV-related HCC, *LPCAT1* was upregulated compared with the HCV-related non-HCC counterpart, according to previous gene expression profiling [32]. Intriguingly, Tanaka *et al.* reported that Lpcat 1-4 were upregulated in a mouse NASH model [33]. In this study, we could acquire a certain range of findings. However, the affected PCs were partially different among HCV, HBV, and non-virus-related HCC. Each HCC accumulates many kinds of genetic abnormalities over time and the phenotypes are quite different, even in the case of the same initiator.

Taking these results into account, we consider LPCAT1 as a potent target molecule to inhibit HCC progression. Since side effects, such as depressed production of pulmonary surfactant, can arise in the case of systemic administration, we should

Please cite this article in press as: Morita Y et al. Lysophosphatidylcholine acyltransferase 1 altered phospholipid composition and regulated hepatoma progression. J Hepatol (2013), http://dx.doi.org/10.1016/j.jhep.2013.02.030

Research Article

consider a focused administration route, such as transcatheter arterial chemoembolization, to explore the feasibility of anti-LPCAT1 drug for clinical applications.

In conclusion, we elucidated altered phospholipid distribution in HCC caused by LPCAT1 overexpression. LPCAT1 could influence HCC proliferation, migration, and invasion.

Financial support

Grant-in-Aid for Scientific Research on Priority Areas at Lipid Machinery, grant from Ministry of Health, Labour and Welfare, Japan to M.S., and Grant-in-Aid for Young Scientists (B) to Y.M.

Conflict of interest

The authors who have taken part in this study declared that they do not have anything to disclose regarding funding or conflict of interest with respect to this manuscript.

Supplementary data

Supplementary data associated with this article can be found, in the online version, at http://dx.doi.org/10.1016/j.jhep.2013.02.030.

References

[1] Jemal A, Bray F, Center MM, Ferlay J, Ward E, Forman D. Global cancer statistics. CA Cancer J Clin 2011;61:69–90.
[2] Bosch FX, Ribes J, Diaz M, Cleries R. Primary liver cancer: worldwide incidence and trends. Gastroenterology 2004;127:S5–S16.
[3] Yamashita T, Honda M, Takatori H, Nishino R, Minato H, Takamura H, et al. Activation of lipogenic pathway correlates with cell proliferation and poor prognosis in hepatocellular carcinoma. J Hepatol 2009;50:100–110.
[4] Stoeckli M, Chaurand P, Hallahan DE, Caprioli RM. Imaging mass spectrometry: a new technology for the analysis of protein expression in mammalian tissues. Nat Med 2001;7:493–496.
[5] Shimma S, Sugiura Y, Hayasaka T, Zaima N, Matsumoto M, Setou M. Mass imaging and identification of biomolecules with MALDI-QIT-TOF-based system. Anal Chem 2008;80:878–885.
[6] Schwamborn K, Caprioli RM. Molecular imaging by mass spectrometry – looking beyond classical histology. Nat Rev Cancer 2010;10:639–646.
[7] Morita Y, Ikegami K, Goto-Inoue N, Hayasaka T, Zaima N, Tanaka H, et al. Imaging mass spectrometry of gastric carcinoma in formalin-fixed paraffin-embedded tissue microarray. Cancer Sci 2010;101:267–273.
[8] Han EC, Lee YS, Liao WS, Liu YC, Liao HY, Jeng LB. Direct tissue analysis by MALDI-TOF mass spectrometry in human hepatocellular carcinoma. Clin Chim Acta 2011;412:230–239.
[9] Le Faouder J, Laouirem S, Chapelle M, Albuquerque M, Belghiti J, Degos F, et al. Imaging mass spectrometry provides fingerprints for distinguishing hepatocellular carcinoma from cirrhosis. J Proteome Res 2011;10:3755–3765.
[10] Hayasaka T, Goto-Inoue N, Sugiura Y, Zaima N, Nakanishi H, Ohishi K, et al. Matrix-assisted laser desorption/ionization quadrupole ion trap time-of-flight (MALDI-QIT-TOF)-based imaging mass spectrometry reveals a layered distribution of phospholipid molecular species in the mouse retina. Rapid Commun Mass Spectrom 2008;22:3415–3426.
[11] Wong JW, Cagney G, Cartwright HM. SpecAlign – processing and alignment of mass spectra datasets. Bioinformatics 2005;21:2088–2090.
[12] Murakami M, Taketomi Y, Miki Y, Sato H, Hirabayashi T, Yamamoto K. Recent progress in phospholipase A(2) research: from cells to animals to humans. Prog Lipid Res 2011;50:152–192.
[13] Moriya K, Todoroki T, Tsutsumi T, Fujie H, Shintani Y, Miyoshi H, et al. Increase in the concentration of carbon 18 monounsaturated fatty acids in the liver with hepatitis C: analysis in transgenic mice and humans. Biochem Biophys Res Commun 2001;281:1207–1212.
[14] Lim K, Han C, Dai Y, Shen M, Wu T. Omega-3 polyunsaturated fatty acids inhibit hepatocellular carcinoma cell growth through blocking beta-catenin and cyclooxygenase-2. Mol Cancer Ther 2009;8:3046–3055.
[15] Kennedy EP, Weiss SB. The function of cytidine coenzymes in the biosynthesis of phospholipides. J Biol Chem 1956;222:193–214.
[16] Lands WE. Metabolism of glycerolipides; a comparison of lecithin and triglyceride synthesis. J Biol Chem 1958;231:883–888.
[17] Shindou H, Shimizu T. Acyl-CoA: lysophospholipid acyltransferases. J Biol Chem 2009;284:1–5.
[18] Nakanishi H, Shindou H, Hishikawa D, Harayama T, Ogasawara R, Suwabe A, et al. Cloning and characterization of mouse lung-type acyl-CoA: lysophosphatidylcholine acyltransferase 1 (LPCAT1). Expression in alveolar type II cells and possible involvement in surfactant production. J Biol Chem 2006;281:20140–20147.
[19] Agarwal AK, Sukumaran S, Bartz R, Barnes RI, Garg A. Functional characterization of human 1-acylglycerol-3-phosphate-O-acyltransferase isoform 9: cloning, tissue distribution, gene structure, and enzymatic activity. J Endocrinol 2007;193:445–457.
[20] DeLong CJ, Baker PR, Samuel M, Cui Z, Thomas MJ. Molecular species composition of rat liver phospholipids by ESI-MS/MS: the effect of chromatography. J Lipid Res 2001;42:1959–1968.
[21] Mitchell TW, Ekroos K, Blanksby SJ, Hulbert AJ, Else PL. Differences in membrane acyl phospholipid composition between an endothermic mammal and an ectothermic reptile are not limited to any phospholipid class. J Exp Biol 2007;210:3440–3450.
[22] Aboagye EO, Bhujwalla ZM. Malignant transformation alters membrane choline phospholipid metabolism of human mammary epithelial cells. Cancer Res 1999;59:80–84.
[23] Mansilla F, da Costa KA, Wang S, Kruhoffer M, Lewin TM, Orntoft TF, et al. Lysophosphatidylcholine acyltransferase 1 (LPCAT1) overexpression in human colorectal cancer. J Mol Med 2009;87:85–97.
[24] Taraboletti G, Perin L, Bottazzi B, Mantovani A, Giavazzi R, Salmona M. Membrane fluidity affects tumor-cell motility, invasion and lung-colonizing potential. Int J Cancer 1989;44:707–713.
[25] Harayama T, Shindou H, Ogasawara R, Suwabe A, Shimizu T. Identification of a novel noninflammatory biosynthetic pathway of platelet-activating factor. J Biol Chem 2008;283:11097–11106.
[26] Aponte M, Jiang W, Lakkis M, Li MJ, Edwards D, Albitar L, et al. Activation of platelet-activating factor receptor and pleiotropic effects on tyrosine phospho-EGFR/Src/FAK/paxillin in ovarian cancer. Cancer Res 2008;68:5839–5848.
[27] Diamond DL, Syder AJ, Jacobs JM, Sorensen CM, Walters KA, Proll SC, et al. Temporal proteome and lipidome profiles reveal hepatitis C virus-associated reprogramming of hepatocellular metabolism and bioenergetics. PLoS Pathog 2010;6:e1000719.
[28] Kim KH, Shin HJ, Kim K, Choi HM, Rhee SH, Moon HB, et al. Hepatitis B virus X protein induces hepatic steatosis via transcriptional activation of SREBP1 and PPARgamma. Gastroenterology 2007;132:1955–1967.
[29] Puri P, Baillie RA, Wiest MM, Mirshahi F, Choudhury J, Cheung O, et al. A lipidomic analysis of nonalcoholic fatty liver disease. Hepatology 2007;46:1081–1090.
[30] Steiling H, Muhlbauer M, Bataille F, Scholmerich J, Werner S, Hellerbrand C. Activated hepatic stellate cells express keratinocyte growth factor in chronic liver disease. Am J Pathol 2004;165:1233–1241.
[31] Mas VR, Maluf DG, Archer KJ, Yanek KC, Fisher RA. Angiogenesis soluble factors as hepatocellular carcinoma noninvasive markers for monitoring hepatitis C virus cirrhotic patients awaiting liver transplantation. Transplantation 2007;84:1262–1271.
[32] De Giorgi V, Monaco A, Worchech A, Tornesello M, Izzo F, Buonaguro L, et al. Gene profiling, biomarkers and pathways characterizing HCV-related hepatocellular carcinoma. J Transl Med 2009;7:85.
[33] Tanaka N, Matsubara T, Krausz KW, Patterson AD, Gonzalez FJ. Disruption of phospholipid and bile acid homeostasis in mice with nonalcoholic steatohepatitis. Hepatology 2012;56:118–129.

Please cite this article in press as: Morita Y et al. Lysophosphatidylcholine acyltransferase 1 altered phospholipid composition and regulated hepatoma progression. J Hepatol (2013), http://dx.doi.org/10.1016/j.jhep.2013.02.030

第64巻第6号 2013年12月15日発行（年6回2・4・6・8・10・12月の15日発行） 1999年3月1日第三種郵便物認可
ISSN 0370-9531 Seitai no Kagaku

生体の科学

SEITAI NO KAGAKU

Vol.64 No.6 2013 Nov.-Dec.

［特集］顕微鏡で物を見ることの新しい動き

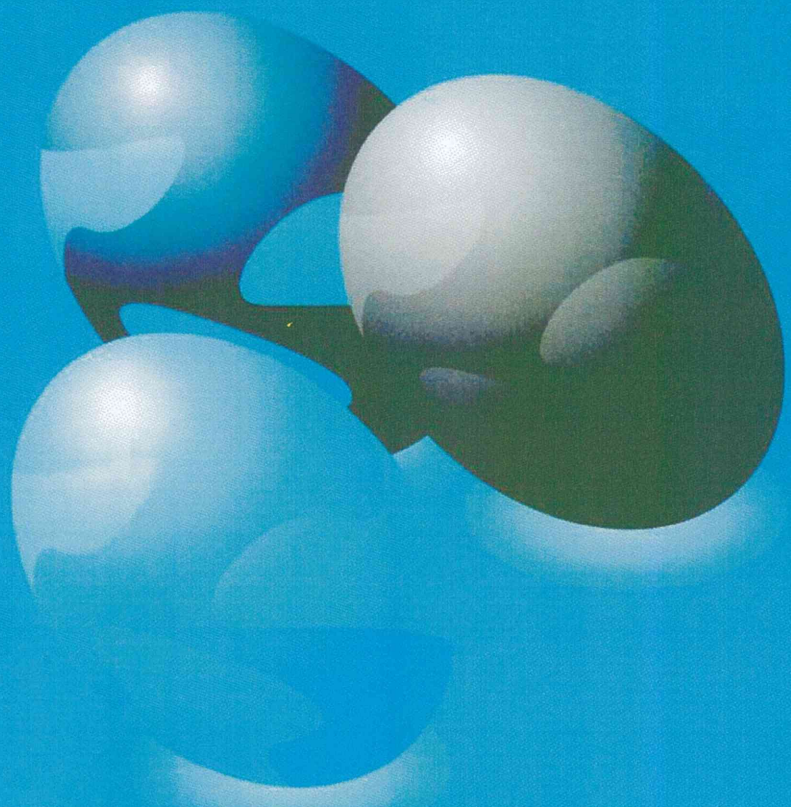

公益財団法人金原一郎記念医学医療振興財団／医学書院

生体の科学　64(6):614-620, 2013

特集　顕微鏡で物を見ることの新しい動き

質量顕微鏡法を用いた生体組織解析

佐野圭吾　瀬藤光利

質量顕微鏡は物質の同定や構造決定に力を発揮する質量分析法と，微細構造解析を行う顕微鏡法を融合させた解析装置である。質量分析によって得られる生化学的情報と位置情報を組み合わせることにより，検出された質量ごとの分布を可視化する質量イメージングを行うことが可能であり，質量イメージング装置の中でイメージングの解像度が肉眼解像度(100 μm)を上回るものを特に質量顕微鏡と言う。質量顕微鏡は物質の質量を直接検出するので抗体やプローブなどによる標識を必要としない。このため対象物質を限定することなく，未知の物質も含めた数千に及ぶ生体分子の検出・同定が可能である。この特徴は，これまで見ることのできなかった脂質や低分子化合物の生体内分布についての新たな知見をもたらしている。本稿では質量顕微鏡の原理について説明すると共に，質量顕微鏡によって得られた生体組織解析の知見や今後の展望について紹介する。

質量顕微鏡のための質量分析法

光学観察を行い試料のイオン化を行うイオン化部と，質量分析のための装置からなる質量分析部によって構成される(図1)。質量分析法は原子，分子，クラスターなどの粒子をイオン化させ，それらのイオンの質量電荷比(質量/電荷：m/z)に応じて分離・検出し，分子量を分析する手法である。質量分析法におけるイオン化法は様々な手法が用いられている[1]。

質量顕微鏡で最も一般的なイオン化法はマトリックス支援レーザー脱離イオン化(matrix assisted Laser desorption/ionization：MALDI)である。MALDIは2002年にノーベル化学賞を受賞された田中ら[2]と，Hillenkamp，Karasら[3]によって開発された。解析物質を結晶マトリックスによって包み込み，そこにパルスレーザー照射することによって物質をイオン化する方法である。レーザー照射による熱エネルギーがマトリックスに吸収されるため，従来のイオン化法では壊れやすかった分子量10万以上のタンパク質やDNAなどの高分子生体物質の分析が可能となった。MALDIでは解析対象物質に適したマトリックスを選択し，そのマトリックスと試料が緊密に混ざり合って結晶化され，解析対象物質のイオン化が行われやすくなっていることが必要である。さらに質量顕微鏡では解析対象物質の組織内分布を崩さずに塗布することが可能な化合物でなければない。

MALDI以外を用いた質量顕微鏡には二次イオン質量分析(secondary ion mass spectrometry：SIMS)が古くから開発されてきた。SIMSはLieblとHerzogによってアメリカ航空宇宙局(NASA)の補助を受けて1960年代に装置として完成され[4]，試料の表面にビーム状のイオン(一次イオン)を照射し，そのイオンと試料表面の分子・

Analysis of physiological tissue with mass microscopy

Sano Keigo, Setou Mitsutoshi：浜松医科大学医学部 解剖学講座 細胞生物学分野(〒431-3192 静岡県浜松市東区半田山1-20-1)

0370-9531/12/¥500/論文/JCOPY

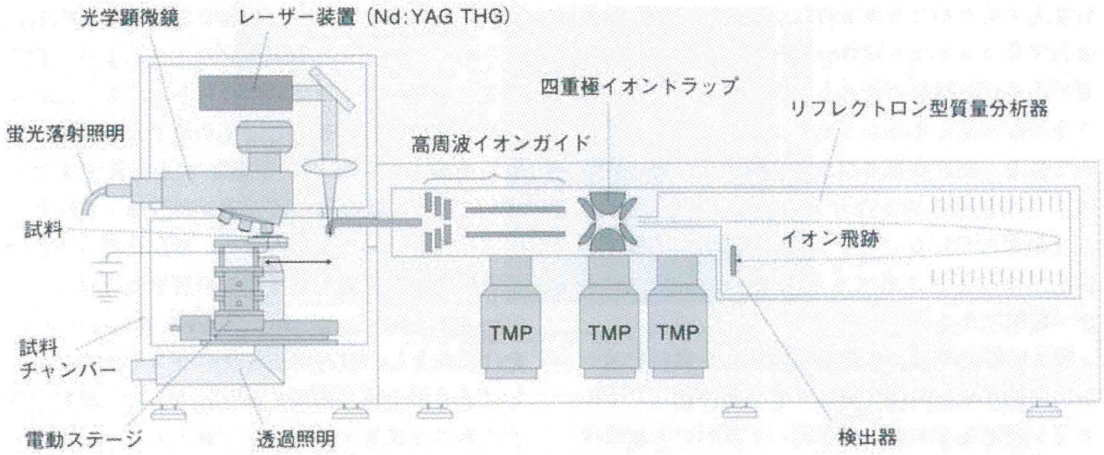

図1　質量イメージング装置（iMScope）概略図

可動式ステージに乗せられた試料は光学観察時には顕微鏡下に，質量分析時にはMALDI法のレーザー照射位置にそれぞれ移動する。イオン化された分子はイオントラップを通った後，TOF-MSにより質量分析が行われる。島津製作所提供。

原子の衝突によってイオン（二次イオン）を発生させる方法である。イオン化の原理上，当初は元素マッピングであり，現在も販売されている装置では m/z 1,000程度までが比較的容易に観測できる範囲である。一方，近年では一次イオン源としてBi（ビスマス；蒼鉛）やAu（金）などの金属クラスターイオンが用いられ，高質量ピークの高感度検出が可能となってきており今後の発展が期待されている。局所でのイオン化が可能であればイオン化法として用いることが可能であるため，マトリックスを用いないレーザー脱離イオン化（Laser desorption/ionization：LDI）[5]，ナノ構造基板を用いる方法[6]，脱離エレクトロスプレーイオン化（desorption electrospray ionisation：DESI）[7]など様々なイオン化法が質量顕微鏡解析のために研究されている。

解析物質はMALDIなどが用いられるイオン化部でイオン化された後，質量分析部にある検出器によって解析される。ここで採用される質量分析方法としては，飛行時間型質量分析法（time of flight mass spectrometry：TOF-MS）が多い。TOF-MSはイオンが質量電荷比（質量/電荷，m/z）に応じて電位差のある空間の移動速度が異なることを利用した方法で，イオン化された試料を電場によって加速し真空中を一定距離飛行させたときの飛行時間を計測することにより質量を測定する分析法である。TOF-MSの特徴として，生成されたイオンを効率的に検出器に導くことができるため高感度であること，原理的に測定できる質量範囲に制限がないことが挙げられる。この特徴は生体組織の解析にとって望ましい。生体組織はイオン化効率の違いなど様々な特徴を持った物質が含まれ，高分子と低分子の広範囲の分子量の物質が含まれるからである。

TOF-MS型の一般的なMALDI質量イメージング装置はイオン化部から高真空に保たれているが，質量顕微鏡では大気圧下でイオン化させ真空である質量分析部に運搬する装置も開発されており，後者のほうが生体組織解析には向いている。これは試料を真空中に置いて観察すると揮発しやすい物質は気化してしまい，組織形態も変化してしまう可能性があり，生体組織の微細な構造や生体分子の構造を保ったまま解析するには大気圧下のほうが望ましいからである。ただし，真空下と大気圧下では物質によってはイオン化の効率が同一とは限らず，真空下でイオン化しやすい物質や大気圧下でイオン化しやすい物質があるため注意が必要である[8]。

質量顕微鏡の実際

一般的に対象となるのは薄切切片である。これは質量顕微鏡法で用いるイオン化法は試料表面を